

A surface dielectric barrier discharge non-thermal plasma to induce cell death in colorectal cancer cells

Cite as: AIP Advances **11**, 075222 (2021); <https://doi.org/10.1063/5.0053501>

Submitted: 08 April 2021 • Accepted: 08 July 2021 • Published Online: 22 July 2021

 Wasin Nupangtha,  Chakkrapong Kuensaen,  Athipong Ngamjarujana, et al.



View Online



Export Citation



CrossMark

ARTICLES YOU MAY BE INTERESTED IN

[Perspectives on cold atmospheric plasma \(CAP\) applications in medicine](#)

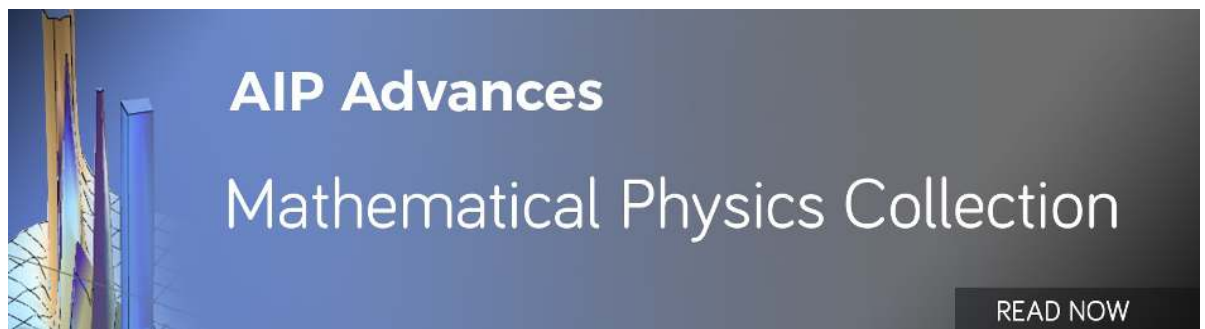
Physics of Plasmas **27**, 070601 (2020); <https://doi.org/10.1063/5.0008093>

[A model of surface dielectric barrier discharge power](#)

Applied Physics Letters **118**, 154102 (2021); <https://doi.org/10.1063/5.0043339>

[Non-thermal plasma multi-jet platform based on a flexible matrix](#)

Review of Scientific Instruments **92**, 083505 (2021); <https://doi.org/10.1063/5.0057438>



AIP Advances
Mathematical Physics Collection

READ NOW

A surface dielectric barrier discharge non-thermal plasma to induce cell death in colorectal cancer cells

Cite as: AIP Advances 11, 075222 (2021); doi: 10.1063/5.0053501

Submitted: 8 April 2021 • Accepted: 8 July 2021 •

Published Online: 22 July 2021



View Online



Export Citation



CrossMark

Wasin Nupangtha,^{1,a)}  Chakkrapong Kuensaen,²  Athipong Ngamjarujana,¹  Siritwadee Chomdej,³ 
and Dheerawan Boonyawan^{1,4,b)} 

AFFILIATIONS

¹Department of Physics and Materials Science, Faculty of Science, Chiang Mai University, Chiang Mai 50200, Thailand

²International College of Digital Innovation, Chiang Mai University, Chiang Mai 50200, Thailand

³Department of Biology, Faculty of Science, Chiang Mai University, Chiang Mai 50200, Thailand

⁴Plasma and Beam Physics Research Center, Chiang Mai University, Chiang Mai 50200, Thailand

^{a)} Author to whom correspondence should be addressed: wasin_nu@cmu.ac.th

^{b)} Electronic mail: dheerawan.b@cmu.ac.th

ABSTRACT

A novel coaxial surface dielectric barrier discharge (SDBD) non-thermal atmospheric pressure plasma device, driven by a 35.7-kHz DC pulse and adjustable by a pulse-width modulation, was developed in this study and preliminarily tested for its killing effects of a cancer cell type. This study was divided into three phases, namely, air phase, liquid phase, and cell phase. First, the electrical characteristics and emissions were examined. Two-beam UV-LED absorption spectroscopy was also newly developed to measure the absolute hydroxyl radical (OH[•]) density in the filamentary discharge. Then, the effects of energy doses and treatment durations on three types of liquids and on the colorectal adenocarcinoma cell, SW620, were examined. From Lissajous figures (Q-V plot), the developed SDBD possesses the maximum power density and energy dose of $0.33 \pm 0.05 \text{ W/cm}^2$ and $19.5 \pm 3.00 \text{ J/cm}^2$, respectively, when the voltage was set at 3.44 kV and the power at 115 mW. From two-beam UV-LED absorption spectroscopy results, the OH[•] density increased by 0.32, 0.58, and $0.86 \times 10^{19} \text{ m}^{-3}$, with operational powers of 29, 58, and 115 mW, respectively, within 1-min treatment. In liquid phases, the plasma device can increase the concentrations of H₂O₂ and NO₂⁻ in a time-dependent manner. Finally, cell-phase studies, including the examination of the cell morphology, cell viability, and gene expression of the SW620 cell, show that the device can time-dependently induce the mortality of the SW620 cell, relevant to the up-regulation of the *Bax/Bcl-2* expression ratio. Taken together, this novel SDBD plasma device shows potential as another alternative for cancer treatment, although further modification is required.

© 2021 Author(s). All article content, except where otherwise noted, is licensed under a Creative Commons Attribution (CC BY) license (<http://creativecommons.org/licenses/by/4.0/>). <https://doi.org/10.1063/5.0053501>

I. INTRODUCTION

The top three cancers that lead to death worldwide are lung, prostate, and colorectal.¹ Selective killing of cancer cells is currently the most important cancer therapy.¹⁻³ Traditional methods used in colorectal cancer treatment include radiotherapy, chemotherapy, and surgery.² However, all these techniques have certain drawbacks. For example, chemotherapy drugs are toxic and kill normal cells while inducing defects, such as tiredness, shortness of breath, bleeding, and infections.⁴ Radiotherapy includes an extremely

condensed beam of radiation that attacks normal cells, and surgery can only treat a local tumor.^{4,5} Over the past decade, the potential of non-thermal atmospheric pressure plasmas (NTAPs) has been seen in various biomedical applications, including disinfection, wound treatment, controlling the formation of blood clots, cancer therapy, and skin problems.⁶⁻¹³ NTAPs have physical applications of electromagnetic, ultraviolet (UV), and heat energies.¹⁴ Reactive oxygen and nitrogen species (RONS) have important radicals in the gas phase of NTAPs, such as hydroxyl (OH),¹⁴⁻¹⁶ singlet oxygen (¹O₂),¹⁵⁻¹⁷ superoxide (O₂⁻),¹⁵ hydrogen peroxide (H₂O₂),¹⁶ nitric

oxide (NO),^{17,18} nitrogen dioxide (NO₂),¹⁸ and nitrogen. OH[•] is one of the most important radicals in NTAP discharge and is the main component to form H₂O₂, which is, on its own, considered to be an active molecule in biology.^{18–24}

A new research field within plasma medicine is the plasma activation of liquids.²⁵ Some recent literature has illustrated the use of dielectric barrier discharges (DBDs) as ignited in closed systems with the counter electrode immersed in the liquid.²⁶ Furthermore, DBD plasma can generate precise target areas with filamentary discharges in front of the DBD surface.^{26–28} These filamentous discharges provide a large amount of RONS products within a limited area and without the use of any gas flow.²⁹ There are demands for a system that can create surface dielectric barrier discharge (SDBD) plasma using small electrodes.^{29,30}

Reactive nitrogen species (RNS) are molecules that play a key role in the promotion of apoptotic cancer cell death.³⁰ Short-lived molecules, such as NO, can react with complex biological surroundings, such as cell culture media, and swiftly oxidize to nitrite (NO₂[•]) and nitrate (NO₃[•]) after their rapid diffusion into the liquid media.^{31,32} It has been known from previous studies that nitrite (NO₂[•]) can play curatively and most likely an intracellular role for NO.³¹ Likewise, the cellular production of the reactive oxygen species (ROS) O₂^{•-} and H₂O₂ promotes the formation of other radicals, such as OH[•] and ONOO[•], which induce oxidative stress and may play a critical role in oncogenesis.³³

This work develops an SDBD device and characterizes its electrical properties and optical emissions in order to use it as a tool to generate an effective amount of RONS. Additionally, two-beam UV-LED absorption spectroscopy is developed to provide the accuracy in measuring the absolute OH[•] density. The RONS complexity of solutions treated with SDBD plasma is then examined. Finally, the biological effects of the treatment of SDBD plasma on SW620 are investigated, i.e., changes in the cell morphology, cell viability, and gene expression.

II. METHODOLOGY

A. Fabrication and experimental setup of the SDBD plasma device

The experimental setup comprised of a discharge part, power supply, and a measurement system, as shown in Fig. 1(a). The filamentary discharge was generated with the surrounding air under ambient pressure. The coaxial copper rod (3 mm diameter) acted as a high voltage electrode and was inserted into an insulator material (ULTEM 1000) with a diameter of 6 mm. The dielectric barrier of the SDBD device was a 0.5-mm thick macro-machinable glass-ceramic on the closed side. The electrode system was powered with a kHz-DC pulse-width modulation. The voltage probe was placed between the stainless mesh ground electrode and the ground as a diagnostic to measure the power dissipation and image the profiles using the Lissajous figure method (Q–V plots). The discharge/charge was determined from the voltage across the 1 μF capacitor, which was measured using an HV probe (Tektronix, P6015A, 75 MHz). The Lissajous figure (Q–V plots) is derived from two channels. The first one is a high voltage probe (4 kV), and the other is the 0.1 μF capacitor (C_{probe}) used to determine the voltage decrease (V_{probe}). The instantaneous charge Q is given by $Q = (C_{probe}) \cdot \Delta V$. The average power consumption was evaluated as $Q \cdot \Delta V$ over the entire period T, which was obtained from the number of data splits (N) based on the discharge duration Δt. The dissipated power (E), power (P), and energy dose are expressed as follows:

$$E = \frac{1}{N} \sum_{i=1}^N Q \Delta V, \quad (1)$$

$$P = \frac{1}{N^2 \Delta t} Q \cdot \Delta V, \quad (2)$$

$$\text{Energy dose} = \left(\frac{Pt}{\text{Area}} \right) \text{J/cm}^2. \quad (3)$$

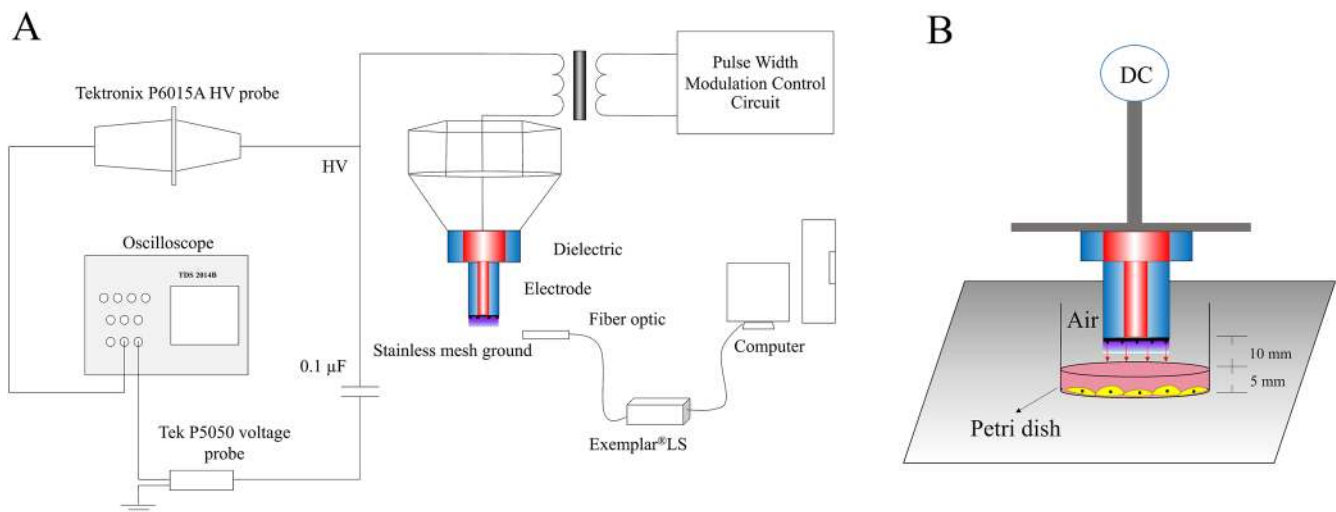


FIG. 1. (a) Schematic diagram of the experimental setup showing the plasma system operated by the DC pulse and (b) an illustration of the ignited SDBD plasma head on the cancer cell specimens.

Next, the configuration of the plasma source treatment for cancer cells in a cell culture medium is shown in Fig. 1(b). The media height was set as 2 mm from the bottom of the Petri dish, and the distance between the plasma device and the top of the media surface was set as ~10 mm as the optimal condition for the plasma treatment of the SDBD device.

B. Hydroxyl radical density measurements

The SDBD was always controlled in an ambient air environment under atmospheric pressures. The SDBD device was placed along the y -axis (Fig. 2) and without surrounding objects to assure the lowest interference from the airflow. To obtain the absorbance $A(\lambda)$ of the OH \cdot band (X²Π-AΣ²), the experimental requirement is to evaluate the incident $I_0(\lambda)$ and transmitted $I_T(\lambda)$ spectral intensities. Briefly, a beam from a light-emitting diode (LED) passes through the absorbing plasma medium and is captured with a spectrograph equipped with a charge-coupled device (CCD) camera. The above-mentioned parameters are calculated as follows:

$$T(\lambda) = \exp(-A(\lambda)) = \frac{I_{(L+P)} - I_P}{I_{(L+P)-ref} - I_{P-ref}}, \quad (4)$$

$$n = -\frac{1}{\sigma L} \left(\frac{I_T(\lambda)}{I_0(\lambda)} \right). \quad (5)$$

Four spectra are needed to measure the transmittance as follows: (1) light source with plasma on the (I_{L+P}) intensities, (2) light source only (I_L), (3) plasma emission only (I_P), and (4) background signal (I_{BG}). The intensity values of the reference beam ($I_{(L+P)-ref}$, I_{P-ref} , I_{L-ref} , and I_{BG-ref}) provide reduced fluctuating signals in the experimental setup. The primary result is the spectral transmittance, $T(\lambda)$. The final forms of the expression according to Beer-Lambert's law are given by Eq. (5), where n is the density, σ is the absorbing cross-sectional area of OH \cdot and is $\sim 1.2 \times 10^{-16}$ cm²,³⁴ and L is the SDBD plasma spatial depth at 6 mm. The two-beam UV-LED absorption setup is in the Mach-Zehnder configuration, as shown in Fig. 2. The UV-LED light source (DUV310-HL5NR) has a spectrum with a center wavelength of $\lambda = 310$ nm and a full width at half-maximum (FWHM) of $\Delta\lambda = 15$ nm.²³ This source is driven by

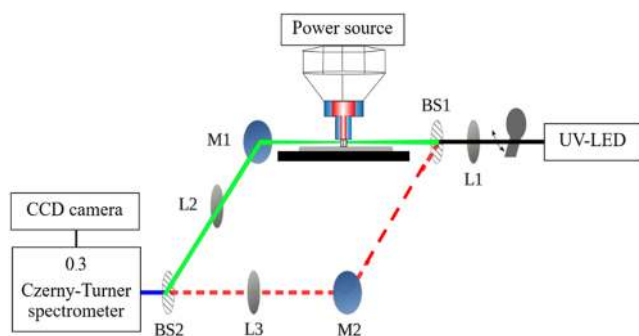


FIG. 2. Diagram of the two-beam UV-LED absorption setup. The red dashed and green solid lines represent the probe beam and the reference beam, respectively.

the controlled supply unit of the current/power (Thorlabs, LTC100) and consumed ~40 mA.

C. H₂O₂ and NO₂⁻ concentration measurements

1 ml of deionized water (DI) water, phosphate buffer saline (PBS), and Dulbecco's Modified Eagle Medium (DMEM) culture medium were treated for 12 min with plasma Lv. 3 and then measured for the concentration of H₂O₂ and NO₂⁻ using the spectroquant hydrogen peroxide test. Later, the DMEM culture medium was plasma-treated for varying durations and measured for the concentrations of H₂O₂ and NO₂⁻. The measurement protocol is to use the hydrogen peroxide kit composed of reagents H₂O₂-1 and H₂O₂-2. First, we prepared reagent H₂O₂-1 at 0.50 ml and pipetted it into a test tube. Then, a sample of 8 ml was added with a pipette and mixed. Finally, reagent H₂O₂-2 at 0.50 ml was added and mixed. After waiting for 10 min, the sample was filled into a 10 mm quartz cuvette. Theoretically, the formation of phenanthroline from the oxidation reaction [copper (II) ions to copper (I) ions] was observed, which results in the formation of an orange color that can be measured photometrically at 445 nm.³⁵ Second, nitrite (NO₂⁻) was detected using the Griess assay (Spectroquant, Merck Millipore, USA). The measurement protocol includes taking the nitrite kit composed of reagent NO₂-1 and sulfanilic acid. First, we prepared a sample of 5 ml and pipetted it into a test tube. Then, the sulfanilic acid solution was added with a pipette and mixed. Finally, one level blue microspoon of reagent N₂O-1 (in the cap of the NO₂-2 bottle) was added and mixed. After 10 min, the sample was filled into the 10 mm quartz cuvette. Theoretically, *N*-(1-naphthyl)-ethylenediamine dihydrochloride (red-violet color) derived from nitrite in the acid solution reacts with sulfanilic acid to form a diazonium salt that can be measured at 525 nm.³⁶ The samples were analyzed within 12 min of plasma exposure. All tests were performed with an UV-vis spectrophotometer (Spectroquant Pharo 100).

D. Cell culture and plasma treatment

Human colorectal cancer epithelial cells, SW620, as derived from lymph node metastasis were cultured in Dulbecco's Modified Eagle Medium (DMEM) with a high glucose level and supplemented with 10% Fetal Bovine Serum (FBS, Thermo Fisher Scientific, USA) and 1X Antibiotic-Antimycotic solution (Thermo Fisher Scientific, USA) in a humidified atmosphere containing 5% CO₂ at 37 °C. Before the experiments, the cells were removed and 1.2×10^5 cells were seeded into six-well plates and incubated for 24 h at 37 °C. The cells were then washed with phosphate-buffered saline (PBS), and 650 μl of fresh culture medium was added to the cells. The cells were treated at varying times of 0 (untreated), 3, 6, 9, and 12 min with plasma Lv. 3.

E. Cell viability measurements using MTT assay

To evaluate the cell viability caused by the SDBD plasma, the activity of mitochondrial enzymes was measured using an MTT assay [3-(4,5-dimethylthiazol-2-yl)-2,5-diphenyl-2H-tetrazolium bromide]. The SW620 cells were then cultured in six-well plates and incubated at 37 °C. Then, serum-free fresh media were replaced with 1 ml of the old removed media. The cells were finally exposed to plasma treatment under various conditions.

TABLE I. Primer sequences for RT-PCR.

Genes	Forward primer [5'-3']	Reverse primer [5'-3']
18S rRNA	AACGAGACTCTGGCATGCTAACTA	CGCCACTTGTCCCTCTAAGAA
Caspase8	TTGAACCCAAGAGGTCAAGG	ACGGGGTCTTGTCTGTTCAC
Bax	AACATGGAGCTGCAGAGGAT	CAGTTGAAGTTGCCGTCAGA
Bcl-2	CGGAGGCTGGGATGCCTTTG	TTTGGGGCAGGCATGTTGAC

After the plasma-treated media cells at 200 μl were transferred to a 96-well plate for the examination using the MTT assay, they were further incubated for 24 h, and 50 μl of MTT solution in the DMEM (ratio, 1:4) was added into each well. The solution was then further incubated for 4 h at 37 °C, and the media were removed. Then, 150 μl of dimethyl sulfoxide (DMSO) was added, mixed, and incubated for 10 min. Finally, the 96-well plate with the solution was measured for absorbance at 570 nm using a microplate reader (Rayto RT-2100C, USA).

F. mRNA expression by semi-quantitative reverse-transcription PCR (RT-PCR)

To measure the mRNA levels, the cells were extracted for the total RNA using the PureLink RNA Mini kit (Thermo Fisher Scientific, USA). The extracted RNA was then reverse-transcribed into cDNA using the Tetro cDNA synthesis kit (Bioline, UK). The cDNA was amplified for 40 cycles using specific primers (Table I).³⁶ The relative mRNA expression level was determined using the $2^{-\Delta\Delta CT}$ method and standardized to the reference gene of 18s ribosomal RNA.^{36,37}

G. Statistical analysis

Data obtained from the experiments on the three replicated samples were presented as mean \pm standard deviation (SD). The one-factor analysis of variance (ANOVA) was used as a tool to determine different statistics between untreated and treated groups assuming a normal distribution of data. This was followed by Tukey's honestly significant difference (HSD) *post hoc* test. Differences were considered statistically significant at * $p < 0.05$, ** $p < 0.01$, and *** $p < 0.001$.

III. RESULTS

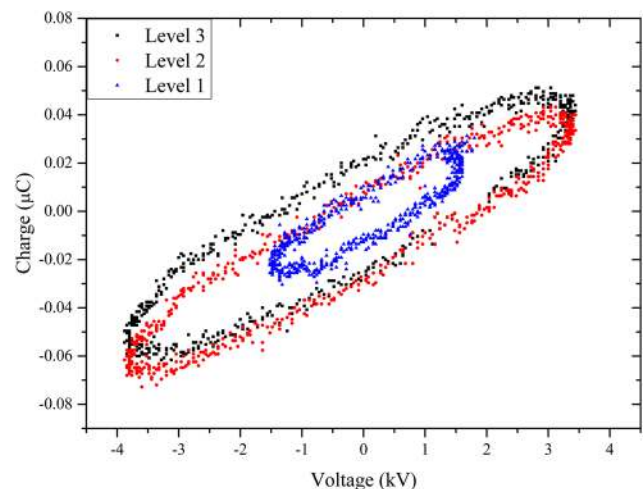
A. Electrical properties and OES measurements of plasma

After the development of surface dielectric barrier discharge (SDBD), the power and electrical properties of plasma were evaluated with an oscilloscope, which were obtained from the area of the Lissajous figure in Fig. 3. The discharge powers were calculated using Eq. (1). An increase in the plasma level significantly affected the electrical parameters of SDBD, which led to a marked increase in the area of the Lissajous figure.

When applying a high voltage of 3.44 kV at a frequency of 35.7 kHz, the plasma can operate at power Lvs. 1–3, which range from 42 to 115 mW. Moreover, the power density and energy dose were evaluated using Eqs. (2) and (3), as shown in Table II. The results show that the power density and energy dose of the SDBD

increase with the DC boost converter rate to the SDBD, which reached maxima at 0.33 W/cm² and 19.5 J/cm² respectively.

The emission spectra in the range of 200–800 nm were recorded by optical emission spectroscopy (OES). This allowed estimating the gas temperature when changing plasma parameters. The setup of the optical emission probe was placed at an angle of 45° with a gap of 5 mm from the plasma discharge. The optical emission spectra indicated the characteristic element spectra, such as NO (220–280 nm), OH⁺ (308.1 nm), N₂ (306–380 nm), and N₂⁺ (391–470 nm), as shown in Fig. 4(a). The transition N₂ (C–B) at 334.27 nm and N₂⁺ (B–X) at 406.24 nm were observed between the wavelengths of 300 and 450 nm. The dominant intensities of plasma Lv. 3 were 22 783 a.u., 13 748 a.u., and 6579 a.u. for N₂ (C–B), OH⁺, and N₂⁺ (B–X), respectively. The gas temperature is the significant parameter to inspect to confirm the heat effect

**FIG. 3.** The C–V characteristic displayed as the Lissajous figure for different plasma-dissipated levels.**TABLE II.** The electrical parameters of the power density and energy dose for different plasma levels.

Condition	Power density (W/cm ²)	Energy dose (J/cm ²)
Lv. 1	0.12 \pm 0.02	7.2 \pm 1.2
Lv. 2	0.17 \pm 0.04	15.3 \pm 2.4
Lv. 3	0.33 \pm 0.05	19.5 \pm 3.0

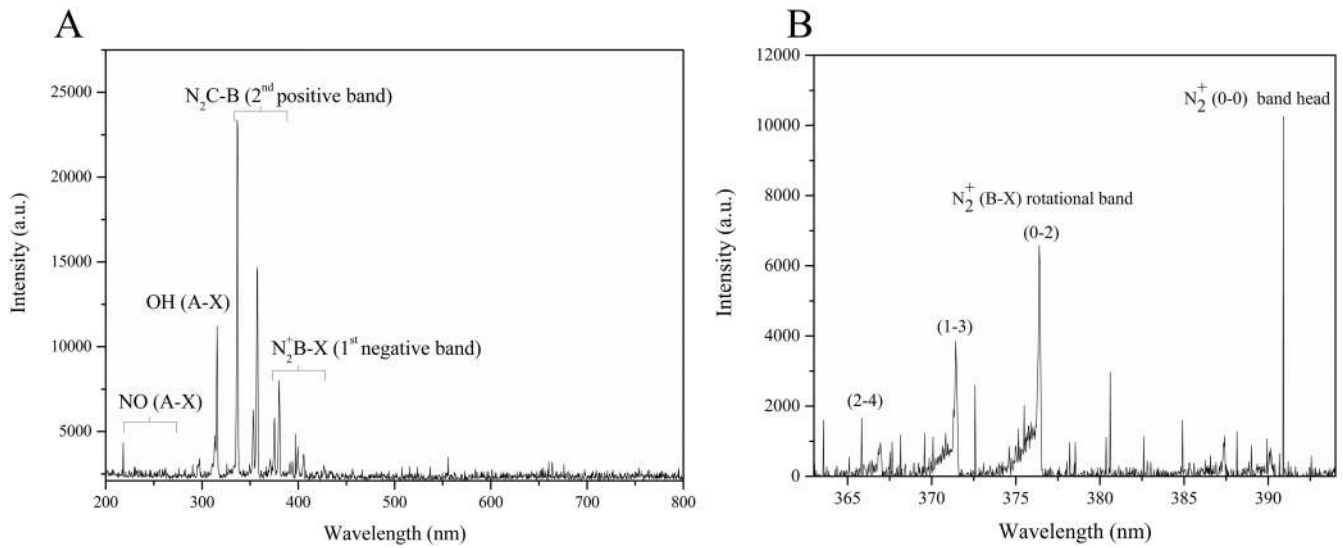


FIG. 4. (a) The optical emission spectra of the SDBD plasma and (b) the emission spectra of the N_2 second positive system ($C^3\Pi-B^3\Pi_g$) between the wavelengths of 360 and 400 nm as ignited at plasma Lv. 3.

of the SDBD device, which was then transferred to the culture media. To obtain the gas temperature, the important parameter was the rotational-vibrational band emission at 391.4 nm.

In this study, the emission spectra of the N_2 second positive band in the transitions of (2-4), (1-3), (0-2), and (0-0) were detected with an AvaSpec-ULS3648 high-resolution spectrometer at a resolution of 0.05 nm and a measured spectrum ranging from 330 to 400 nm, as shown in Fig. 4(b). The rotational band temperature was determined based on Eq. (6) with the left-hand side terms plotted against $j'(j'+1)$. The slope of the curve on the right-hand side term yields the rotational temperature,³⁸

$$\ln \frac{I^{em}}{j'+j''+1} = -\frac{B'vhc}{K_B T} j'(j'+1) + \ln C. \quad (6)$$

There are seven parameters needed to estimate the gas temperature: (1) the intensity of the transition for the rotational level (I^{em}), (2) and (3) the rotational quantum numbers of the upper and lower electronic states (j' and j''), (4) the speed of light in vacuum (C), (5) the statistical weight of the upper level ($B'v$), (6) Planck's constant (hc), and (7) Boltzmann's constant (K_B). To determine the gas temperature, the rotational band of N_2^+ was used for plasma discharge at ambient pressure, where nitrogen molecules exchange rotational energy quicker with heavy particles than with electrons. Consequently, T_r can be considered as an estimate of the gas temperature, T_g . The rotational temperature was around 345 K from a linear fit of plasma Lv. 3, as shown in Fig. 5.³⁹⁻⁴²

B. Hydroxyl radical density

The important species that appear between the plasma and water surface are hydroxyl radicals (OH^\cdot). The spectra of the probe beam (ROI 1) and reference beam (ROI 2) were resolved under plasma Lv. 3 by a 1-min operation, as seen in Fig. 6. We measured

the transmission ratio (I_T/I_0) of the two-beam UV as caused by OH^\cdot , which provided four intensities, namely, I_{L+P} , I_P , I_L , and I_{BG} , as shown in Fig. 7(a). It is noted that the UV transmission I_T can be obtained by comparing the emission profiles from the intensities of the plasma and LED (I_{L+P}) with that of the plasma (I_P).

The reference LED (I_L) is shown in the lower line (blue), while the background is represented in the bottom line (pink). The emission profiles of I_{L+P} and I_P appear strongly around 308–309 nm, which indicates that OH^\cdot generation occurred. Figure 7(b) shows the hydroxyl radical density vs power plot with a time duration of

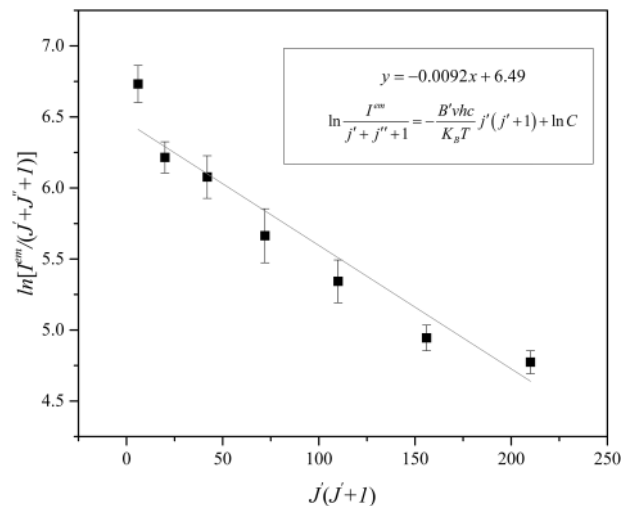


FIG. 5. Linear fit of the rotational temperature using the spectral intensity at plasma Lv. 3.

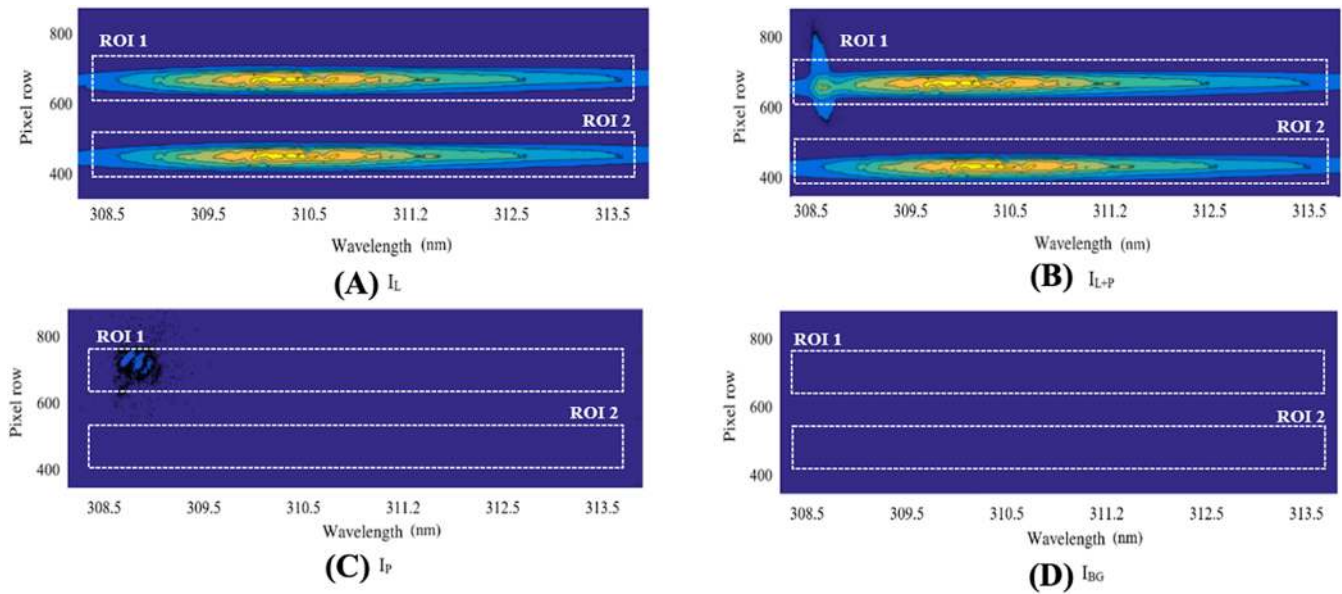


FIG. 6. Images showing the probe beam [pixel row, 770–920 (top)] and reference beam [pixel row, 430–550 (bottom)] intensities. The different colors indicate the scale from max to min (yellow to blue). (a) Light source only (I_L). (b) Light source with plasma on the intensities (I_{L+P}). (c) Plasma emission only (I_P). (d) Background signal (I_{BG}).

1 min. The results indicate that the OH^\cdot density increased by 0.32, 0.58, and $0.86 \times 10^{19} \text{ m}^{-3}$, with operational powers of 29, 58, and 115 mW, respectively.

C. Chemical analysis of the solutions

To study the effects of plasma irradiation on the chemical composition of different solutions, deionized water (DI),

phosphate-buffered saline (PBS), and Dulbecco's Modified Eagle Medium (DMEM) were treated with plasma at varying durations and measured to determine the concentrations of H_2O_2 and NO_2^- using a photometric assay. The graph in Fig. 8(a) shows the concentrations of 1.23, 1.37, and 5.17 mg/l for H_2O_2 and 0.01, 0.04, and 0.72 mg/l for NO_2^- in DI, PBS, and DMEM, respectively. It was found that the H_2O_2 and NO_2^- concentrations in the DMEM were significantly higher than in DI and PBS. Next, the effects of the

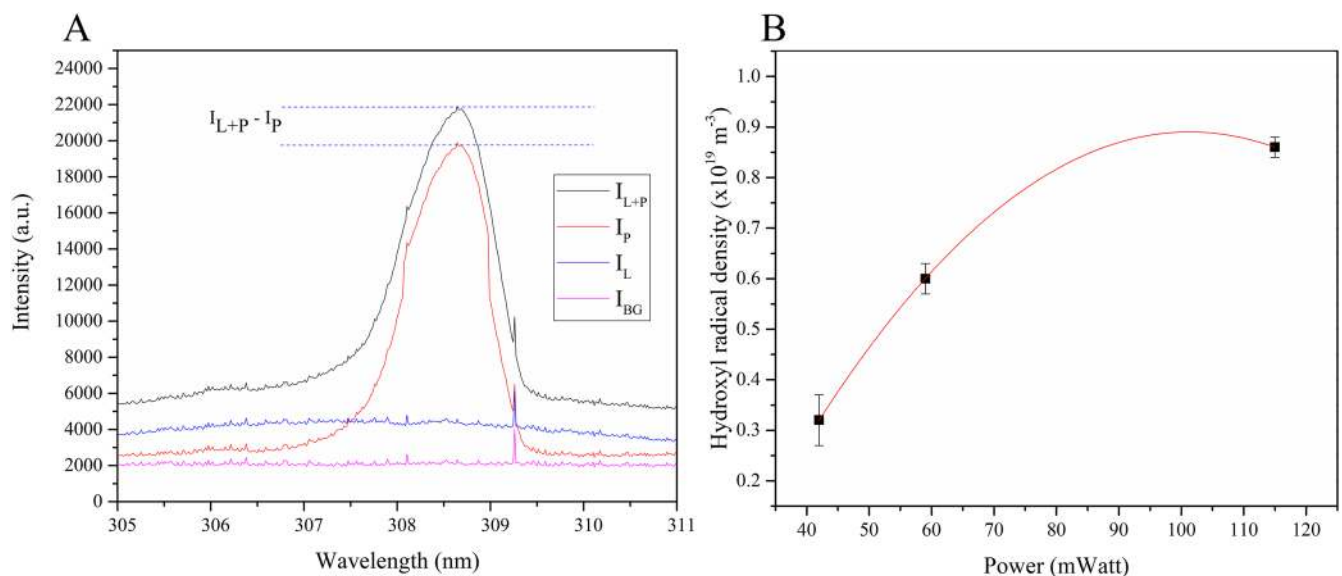


FIG. 7. (a) The emission profile intensities for I_{L+P} , I_P , I_L , and I_{BG} to obtain the OH^\cdot density and (b) OH^\cdot (X) density at RH = 65% for different operating powers.

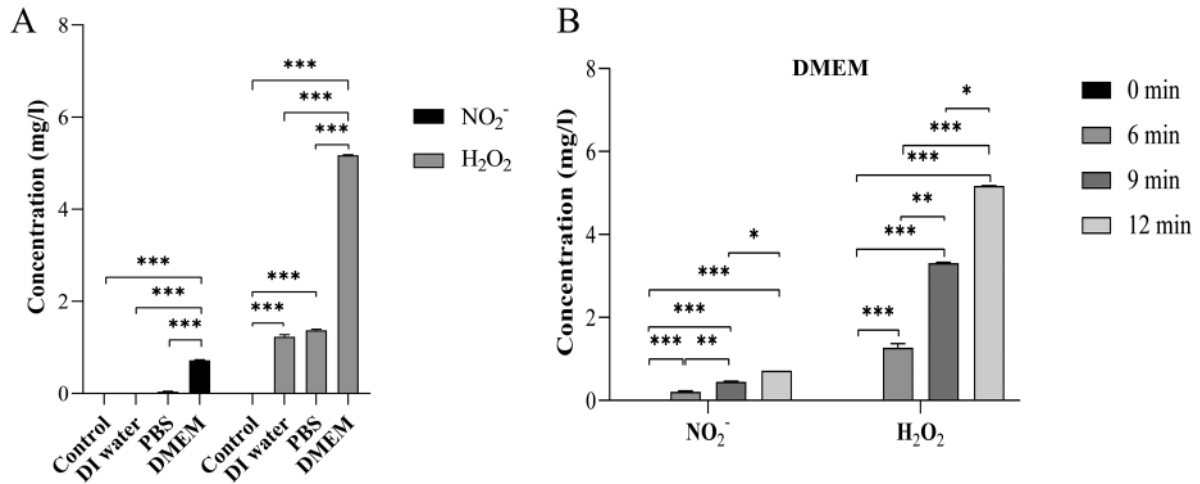


FIG. 8. (a) Concentrations of NO_2^- and H_2O_2 as obtained from three different SDBD-treated liquids (DI water, PBS, and DMEM culture medium) after 12-min plasma Lv. 3 treatment and (b) concentrations of H_2O_2 and NO_2^- in the DMEM culture medium after SDBD plasma Lv. 3 treatment for varying times. Data are presented as mean \pm SD (** $p < 0.001$, * $p < 0.01$, and * $p < 0.05$).

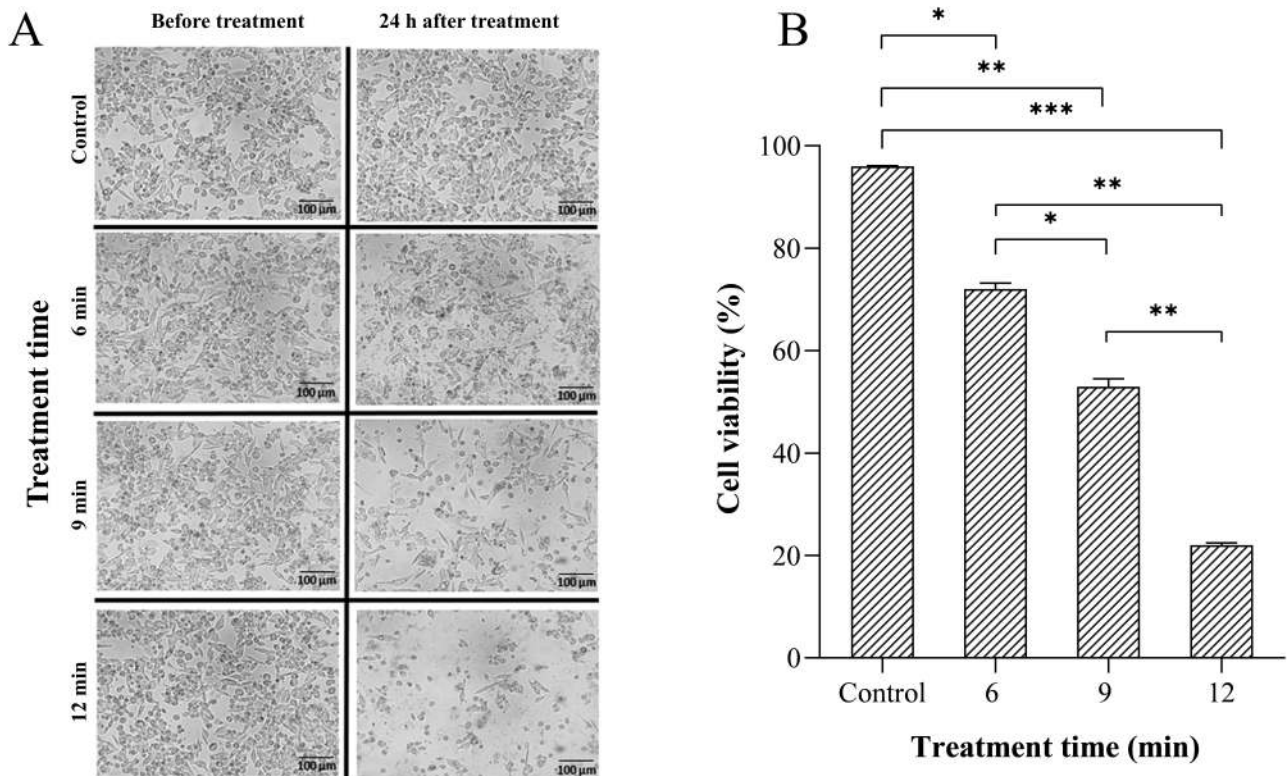


FIG. 9. (a) The morphology of colorectal adenocarcinoma SW620 cells before and after plasma treatment for varying durations. Images were taken at 100 \times magnification. (b) Relative SW620 cell viability after exposure to SDBD plasma Lv. 3 for indicated times. Data were from three different experiments and are shown as mean \pm SD (** $p < 0.001$, * $p < 0.01$, and * $p < 0.05$).

plasma on the DMEM were examined, as shown in Fig. 8(b). The H_2O_2 and NO_2^- concentrations increased significantly with the treatment duration ($p < 0.05$ and $p < 0.001$, respectively).

D. Effects of SDBD plasma on the cell morphology and viability of colorectal adenocarcinoma epithelial cells

The effects of the treatment duration on the cell morphology of the cancerous colorectal adenocarcinoma cell line SW620 were examined. The cells were treated with SDBD plasma for 6–12 min with a plasma energy set to Lv. 3. After post-treatment incubation for 24 h, the SW620 cells were observed under an inverted microscope at 100 \times magnification, as shown in Fig. 9(a). After treatment for 6 min, the cells began to show noticeable detachment compared to untreated samples. The 9- and 12-min treatments caused the cells to severely detach and shrink. In addition, the cell viability was measured using the MTT assay. The results show that the viability of

SW620 cells decreased by ~5%, 28%, 47%, 78%, and 79% after 3, 6, 9-, 12-, and 15-min treatments, respectively.

E. mRNA expression of apoptosis-related genes

The effects of the plasma treatment on the intracellular gene expression of cell-death-related molecules were investigated. The SW620 cells covered in a thin layer of the complete DMEM medium were exposed to the plasma Lv. 3 for varying durations and incubated for 24 h. After the post-treatment incubation, the mRNA levels of the genes of interest were measured using semi-quantitative reverse-transcription polymerase chain reaction (PCR) (RT-PCR). The results shown in Fig. 10(a) indicate that the SW620 cells exposed to plasma for 12 min showed high expression levels of the *Bax* gene and slightly increased levels of the *Caspase 8* expression, whereas the expression of *Caspase 8* genes did not significantly increase after 6- or 9 min-treatment compared to the untreated samples. To determine the cell susceptibility to apoptosis, the *Bcl-2* and *Bax* ratios

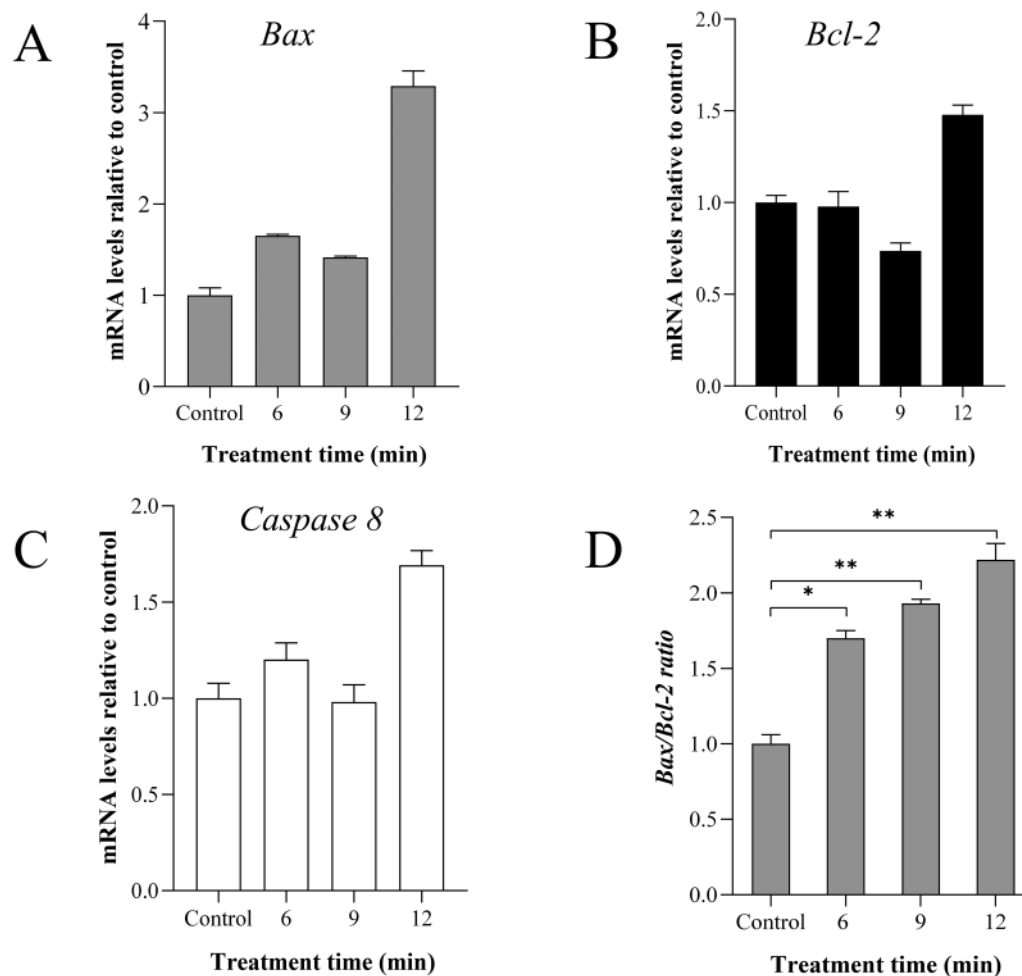


FIG. 10. SW620 cells exposed to SDBD plasma Lv. 3 for varying time durations. The mRNA levels of *Bax* (a), *Bcl-2* (b), and *Caspase 8* (c) genes are shown, and (d) ratios between the expression of *Bax* and *Bcl-2* genes were calculated, relative to the control and normalized with a reference gene. Data were from three different experiments and are shown as mean \pm SD (** $p < 0.01$ and * $p < 0.05$).

were observed under plasma Lv. 3 and at varying treatment durations. The results shown in Fig. 10(b) indicate that the *Bax/Bcl-2* ratio expression resulted in 1.7-fold, 1.93-fold, and 2.2-fold increases after 6-, 9-, and 12-min treatments, respectively.

IV. DISCUSSION

This study characterized the newly developed SDBD plasma device and its optimal condition for operation. This device consists of two important electrodes: the glass-ceramic electrode and the ground electrode. The former is a dielectric-protected powered electrode, while the latter is a mesh of stainless steel. The principle of operation of the SDBD device was recently discussed in detail.⁴³ It is noteworthy that the SDBD device is a perfectly integrated electrical circuit and is thus non-damaging for biomedical applications.^{43,44}

The effects of the plasma device on both chemical and biological substances are usually relevant to the energy dose generated. According to Kalghatgi *et al.*,¹⁴ the DBD plasma treatment, with an energy dose higher than 15 J/cm², can induce 40% cell death in melanoma cancer cells. This is in accordance with our SDBD device, where, at Lv. 3, it produced an energy dose of ~19.5 J/cm² and induced more than 40% mortality after 9-min treatment. In Table III, the effects of cancer cell death induction by other SDBD devices with different plasma systems are also compared.^{45–49} For example, enhancing the NTAP with the temozolomide (TMZ) drug can decrease glioblastoma cancer cells (U87MG) by 40%.⁴⁶ Next, the enhanced anti-melanoma effect was achieved using the NTAP with the anti-FAK antibody conjugated gold nanoparticles to treat melanoma cancer cells, which can reduce melanoma cells by 74%.⁴⁵

This mortality of cancer cells is reported to be mainly related to the density of hydroxyl radicals; thus, we developed the two-beam UV-absorption spectroscopy system to measure the absolute density of hydroxyl radicals in the gas phase. Then, the former densities were compared to the concentrations of hydroxyl radicals measured from the plasma-treated solutions as a way to describe the generation of radicals in the liquid phase. In the experimental

configuration, the distance between the plasma head and the top of the media surface was set as 10 mm as the optimal condition. From a previous study, the diffusion coefficient of OH[•] at atmospheric pressures in ambient air was ~165 ± 20 Torr cm² s⁻¹ at 293 K.⁵⁰ Additionally, short-lived molecules, such as NO, can diffuse into cultured media at 298 K, and their diffusion coefficient of was found to be 2.21 ± 0.04 × 10⁻⁵ cm² s⁻¹.⁵¹

Typically, the plasma dose influences the RONS production. For example, a plasma dose of 3.9 J/cm² can produce a RONS amount of ~2 × 10¹⁷ cm⁻³, as reported by Sensenig *et al.*⁴⁹ The SDBD can produce various RONS species in the gas phase. In particular, NO_x radicals are generated due to the ambient nitrogen gas at ~78%, and the presence of OH[•] is due to natural water vapor in the ambient air environment. The OH[•] density at plasma Lv. 3 is ~8.5 × 10¹⁹ m⁻³ as obtained by two-beam UV-LED absorption spectroscopy [Fig. 7(b)]. It is noted that this value of the OH[•] density is lower by two orders of magnitude compared with the plasma jet technique.⁵²

On the other hand, this value is in relative agreement with the value of 2–7 × 10¹⁹ m⁻³ reported by Martini *et al.*⁵³ at low water molecule contents less than 1% in the employed gas mixture of Ar/O₂ using the DBD technique. In general, OH[•] in the gas phase can diffuse into the liquid phase, which can be transformed into H₂O₂ and is considered the most important RONS that contributes to plasma damage to cancer cells. The short-lived species, such as OH[•], can be transformed into H₂O₂ (long-living species) in the liquid phase via recombination reactions. As shown in a previous study, the presence of H₂O₂ in the liquid phase of ~70% is produced by indirect plasma processes.⁵⁴ The H₂O₂ reactions are generated using the following equations:⁵⁵

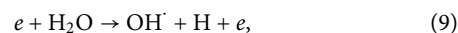
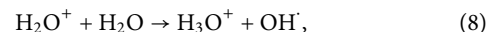
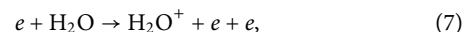
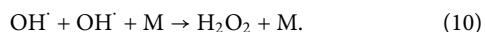
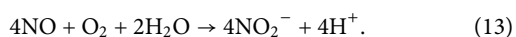


TABLE III. Comparison of the different non-thermal plasma techniques in cancer therapy.

	Method of treatment	Cell types	Electrical parameter	Treatment time (min)	% Induced mortality (%)
Plasma jet technique	Plasma with temozolomide (TMZ) ⁴⁶	Glioblastoma cells (U87MG)	0.6 J/cm ² in 60 s	3	75
	Plasma jet ⁴⁸	Human lung (A549)	2.54 GHz, 5–8 W	3	70
	Plasma jet ⁴⁷	Human breast cancer cell line (MDA-MB-231)	2–5 kV, 30 kHz	2	75
Dielectric barrier discharge	Floating dielectric barrier discharge (FDBD) ⁴⁹	Melanoma cell	60 J/cm ² in 60 s	4	80
	Dielectric barrier discharge with the anti-FAK antibody-conjugated gold nanoparticles (DBD + FAK-GNP) ⁴⁵	Melanoma cell	5 kV, 22 kHz	1	74
	Surface dielectric barrier discharge (SDBD)	Colorectal cancer cell	19.5 J/cm ² in 60 s	12	78



The SDBD treatment with plasma Lv. 3 on DI water, PBS, and DMEM culture medium was performed to induce changes in the RONS concentrations within different liquids and different treatment durations. The results shown in Fig. 8(b) indicate that the NO_2^- concentrations in SDBD-treated DI water, PBS, and DMEM increase with the treatment duration. A large amount of NO can be generated in the gas phase after discharge in ambient air. For example, NO_2^- can be generated as NO using the following equations:^{56,57}



From our results, it is significant that the concentrations of hydrogen peroxide and nitrite were higher in the DMEM, and this might be due to its components, which contain 36 items, including amino acids, inorganic salts, and vitamins. On the other hand, PBS containing disodium hydrogen phosphate and sodium chloride can adjust the constant pH and affect the hydrogen peroxide concentration.⁵⁸ This might be the reason why the concentration of hydrogen peroxide induced by the plasma in the DMEM was greater than in PBS solution. The amino acid in the DMEM solution may also react with plasma to produce NO_2^- .

However, whether this SDBD plasma can be effectively used in physiological conditions is an underlying question and needs to be further investigated. Cysteine, one of the amino acids found abundantly in both human blood plasma and DMEM, was reported to consume most of the active species and almost completely eliminate the anti-tumor capacity of the NTAP-treated DMEM on U87 cells.⁵⁹ Although this contradicts our findings that the SDBD-treated DMEM could maintain the generated active species and result in the induction of cell death, we still do not have a concrete evidence to support the idea of its functioning in physiological conditions. Nevertheless, we commit ourselves to further study the effects of this SDBD plasma in physiological conditions.

SW620, a cancerous colorectal adenocarcinoma cell line, was chosen as a model for this study due to its rapid proliferation and strong adhesion.⁶⁰ We examined the effects of SDBD plasma on cell mortality by first considering the cell morphology and cell detachment, which can be counted as primary indicators of cell injury. By this, we confirmed that the plasma Lv. 3 treatment for a duration of 12 min could damage SW620 morphologically. The results of mitochondrial activity using MTT assay also confirmed the cell mortality induced by SDBD plasma.

Despite this, the question of the selectivity capability for cancer killing is still the point of interest for this application. Preliminarily, a keratinocyte cell line, HaCaT, was used as a representative of non-cancerous cells to study the selective killing effects of SDBD plasma. Although this cell type is not a good comparison for the colorectal cell and we did not include these results in the main text, the results could still provide us some helpful direction. From Fig. S1, where SW620 and HaCaT cells were plasma-treated for varying durations and observed under a microscope, it is

evident that HaCaT cells could maintain its morphology and attachment better than SW620 cells after receiving plasma treatment for the same period of time. As after 9-min treatment, the time when both cell types started to detach and shrink, more than ~60% of SW620 cells were affected, while less than ~40% of HaCaT cells were affected. After 12-min treatment, more than 90% of SW620 cells were shrunk or detached, while HaCaT cells showed the comparable percentage of affected cells after being treated for 9 min. In Fig. S2, the cell viability after plasma treatment was measured using the MTT assay. After 6-min treatment, SW620 cells started to show higher mortality than HaCaT cells, and the trend was even more noticeable after 9- and 12-min plasma treatment. These results initially support the concept of selective-killing capability of the novel SDBD device, although thorough studies are mandatory to verify its selectivity capability.

There are theories explaining how plasma treatment results in the mortality of cells. Other than generated UV and electromagnetic fields, it was proposed that high concentrations of NO_2^- and H_2O_2 could damage DNA via indirect chain induction^{25,60,61} by plasma. Second, H_2O_2 and NO_2^- can also transform into peroxy-nitrite ($\text{H}_2\text{O}_2 + 2\text{NO}^- \Rightarrow 2\text{HNOO}^-$),^{1,32} which is a radical capable of causing cancer cells to undergo apoptosis,⁶² which is in accordance with our results on the increased concentrations of H_2O_2 and NO_2^- .

There were also reports speculating the involvement of plasma treatment and the induction of intrinsic and extrinsic apoptosis.⁶³ *Caspase 8* is a cysteine aspartic acid protease, which plays an important role in extrinsic signaling pathways involving death receptors.¹⁶ *Bax* is a *Bcl-2* family protein that is related to the intrinsic signaling pathway of mitochondria membranes in pro-apoptosis processes. *Bax* overexpression can be induced by chemotherapeutic agents.^{64,65} The *Bcl-2* proteins are the primary regulators of the intrinsic apoptotic pathway.⁶⁶ From our results, it is clear that the intrinsic pathway of apoptosis is induced earlier than the extrinsic pathway and the escalation of the *Bax/Bcl-2* ratio, representing the apoptosis tendency, is time-dependent, fitting with the accumulated concentrations of hydrogen peroxide and nitrite. This is in agreement with Hawkins' report,⁶⁶ which demonstrated that SDBD plasma induces apoptosis by shifting the ratios between *Bax* and *Bcl-2*.

Taken together, the developed SDBD plasma device showed potential as a generator of radicals capable of inducing the death of colorectal adenocarcinoma SW620 cells, possibly through the intrinsic pathway of apoptosis. However, whether the device can equivalently function in the physiological conditions is still unclear, and thus, the device is needed to be further tested on either animal's or human's plasma or serum prior to the *in vivo* experiment.

SUPPLEMENTARY MATERIAL

See the [supplementary material](#) for the effects of the SDBD plasma on HaCaT cells as a model of plasma's effects on a non-cancerous cell type.

AUTHORS' CONTRIBUTIONS

W.N. and C.K. contributed equally to this work.

ACKNOWLEDGMENTS

This research was supported by the Science Achievement Scholarship of Thailand (SAST) under the Government of Thailand and the Plasma and Beam Physics (PBP) Research Center, Department of Physics and Material Sciences, and Department of Biology, Faculty of Science, Chiang Mai University. W.N. was supported by Graduate School, Chiang Mai University. C.K. was supported by the CMU Junior Research Fellowship Program (Grant No. JRCMU2564_070).

DATA AVAILABILITY

The data that support the findings of this study are available within the article.

REFERENCES

- 1 S. A. Norberg, W. Tian, E. Johnsen, and M. J. Kushner, *J. Phys. D: Appl. Phys.* **47**(47), 475203 (2014).
- 2 T. Darny, J.-M. Povesle, V. Puech, C. Douat, S. Dozias, and E. Robert, *Plasma Sources Sci. Technol.* **26**(4), 045008 (2017).
- 3 A. Lin, B. Truong, S. Patel, N. Kaushik, E. Choi, G. Fridman, A. Fridman, and V. Miller, *Int. J. Mol. Sci.* **18**(5), 966 (2017).
- 4 G. J. Kim, W. Kim, K. T. Kim, and J. K. Lee, *Appl. Phys. Lett.* **96**(2), 021502 (2010).
- 5 M. Laroussi, S. Mohades, and N. Barezki, *Biointerphases* **10**(2), 029401 (2015).
- 6 A. Shashurin, M. Keidar, S. Bronnikov, R. A. Jurjus, and M. A. Stepp, *Appl. Phys. Lett.* **93**(18), 181501 (2008).
- 7 E. Stoffels, Y. Sakiyama, and D. B. Graves, *IEEE Trans. Plasma Sci.* **36**(4), 1441–1457 (2008).
- 8 G. E. Morfill, M. G. Kong, and J. L. Zimmermann, *New J. Phys.* **11**(11), 115011 (2009).
- 9 A. Shashurin, M. A. Stepp, T. S. Hawley, S. Pal-Ghosh, L. Brieda, S. Bronnikov, R. A. Jurjus, and M. Keidar, *Plasma Processes Polym.* **7**, 294–300 (2010).
- 10 X. Dai, Y. Luo, Y. Xu, and J. Zhang, *Am. J. Cancer Res.* **9**, 1027–1042 (2019); available at <https://pubmed.ncbi.nlm.nih.gov/31218110/>.
- 11 P. Thana, C. Kuensaen, P. Poramapijitwat, S. Sarapirom, L. Yu, and D. Boonyawan, *Surf. Coat. Technol.* **400**, 126229 (2020).
- 12 P. Thana, A. Wijaikhum, P. Poramapijitwat, C. Kuensaen, J. Meerak, A. Ngamjarujana, S. Sarapirom, and D. Boonyawan, *Heliyon* **5**(9), e02455 (2019).
- 13 P. Poramapijitwat, P. Thana, D. Boonyawan, K. Janpong, C. Kuensaen, W. Charentantakul, L. D. Yu, and S. Sarapirom, *Surf. Coat. Technol.* **402**, 126482 (2020).
- 14 S. Kalghatgi, C. M. Kelly, E. Cerchar, B. Torabi, O. Alekseev, A. Fridman, G. Friedman, and J. Azizkhan-Clifford, *PLoS One* **6**(1), e16270 (2011).
- 15 M. Keidar, R. Walk, A. Shashurin, P. Srinivasan, A. Sandler, S. Dasgupta, R. Ravi, R. Guerrero-Preston, and B. Trink, *Br. J. Cancer* **105**(9), 1295–1301 (2011).
- 16 S. Ja Kim, H. Min Joh, and T. H. Chung, *Appl. Phys. Lett.* **103**(15), 153705 (2013).
- 17 S. J. Kim and T. H. Chung, *Sci. Rep.* **6**(1), 20332 (2016).
- 18 S. Reuter, H. Tresp, K. Wende, M. U. Hammer, J. Winter, K. Masur, A. Schmidt-Bleker, and K.-D. Weltmann, *IEEE Trans. Plasma Sci.* **40**(11), 2986–2993 (2012).
- 19 J. Y. Jeong, S. E. Babayan, A. Schütze, V. J. Tu, J. Park, I. Henins, G. S. Selwyn, and R. F. Hicks, *J. Vac. Sci. Technol. A* **17**(5), 2581–2585 (1999).
- 20 P. Bruggeman, G. Cunge, and N. Sadeghi, *Plasma Sources Sci. Technol.* **21**, 035019 (2012).
- 21 T. Verreycken, R. Mensink, R. van der Horst, N. Sadeghi, and P. J. Bruggeman, *Plasma Sources Sci. Technol.* **22**, 055014 (2013).
- 22 Q. Xiong, Z. Yang, and P. J. Bruggeman, *J. Phys. D: Appl. Phys.* **48**(42), 424008 (2015).
- 23 A. Wijaikhum, D. Schröder, S. Schröter, A. R. Gibson, K. Niemi, J. Friderich, A. Greb, V. Schulz-von der Gathen, D. O’Connell, and T. Gans, *Plasma Sources Sci. Technol.* **26**(11), 115004 (2017).
- 24 S. Bekeuschus, A. Lin, A. Fridman, K. Wende, K.-D. Weltmann, and V. Miller, *Plasma Chem. Plasma Process.* **38**(1), 1–12 (2018).
- 25 P. Lukes, E. Dolezalova, I. Sisrova, and M. Clupek, *Plasma Sources Sci. Technol.* **23**, 015019 (2014).
- 26 M. Thiyagarajan, H. Anderson, and X. F. Gonzales, *Biotechnol. Bioeng.* **111**(3), 565–574 (2013).
- 27 S. Zhao, Z. Xiong, X. Mao, D. Meng, Q. Lei, Y. Li, P. Deng, M. Chen, M. Tu, X. Lu, G. Yang, and G. He, *PLoS One* **8**, e73665 (2013).
- 28 S. Yonemori and R. Ono, *Biointerphases* **10**(2), 029514 (2015).
- 29 N. Kurake, H. Tanaka, K. Ishikawa, T. Kondo, M. Sekine, K. Nakamura, H. Kajiyama, F. Kikkawa, M. Mizuno, and M. Hori, *Arch. Biochem. Biophys.* **605**, 102 (2016).
- 30 H. Hara, M. Kobayashi, M. Shiiba, T. Kamiya, and T. Adachi, *J. Clin. Biochem. Nutr.* **65**(1), 16–22 (2019).
- 31 A. Fridman, A. Chirokov, and A. Gutsol, *J. Phys. D: Appl. Phys.* **38**(2), R1–R24 (2005).
- 32 D. B. Graves, *J. Phys. D: Appl. Phys.* **45**(26), 263001 (2012).
- 33 C. Szabó, H. Ischiropoulos, and R. Radi, *Nat. Rev. Drug Discovery* **6**, 662–680 (2007).
- 34 H.-P. Dorn, R. Neuroth, and A. Hofzumahaus, *J. Geophys. Res.: Atmos.* **100**(D4), 7397–7409, <https://doi.org/10.1029/94jd03323> (1995).
- 35 A. Azzariti, R. M. Iacobazzi, R. Di Fonte, L. Porcelli, R. Gristina, P. Favia, F. Fracassi, I. Trizio, N. Silvestris, G. Guida, S. Tommasi, and E. Sardella, *Sci. Rep.* **9**(1), 4099 (2019).
- 36 S. Rozen and H. Skaletsky, *Methods Mol. Biol.* **132**, 365–386 (2000).
- 37 M. W. Pfaffl, *Nucleic Acids Res.* **29**(9), e45 (2001).
- 38 S. B. Bayram, P. T. Arndt, and M. V. Freamat, *Am. J. Phys.* **83**(10), 867–872 (2015).
- 39 F. Cramarossa and G. Ferraro, *J. Quant. Spectrosc. Radiat. Transfer* **14**(2), 159–163 (1974).
- 40 J. Janča, L. Skrička, and A. Brablec, *Plasma Chem. Plasma Process.* **13**(3), 567–577 (1993).
- 41 G. Gardet, G. Moulard, M. Courbon, F. Rogemond, and M. Druetta, *Meas. Sci. Technol.* **11**(4), 333–341 (2000).
- 42 N. Britun, M. Gaillard, A. Ricard, Y. M. Kim, K. S. Kim, and J. G. Han, *J. Phys. D: Appl. Phys.* **40**(4), 1022–1029 (2007).
- 43 G. Fridman, M. Peddinghaus, H. Ayan, A. Fridman, M. Balasubramanian, A. Gutsol, A. Brooks, and G. Friedman, *Plasma Chem. Plasma Process.* **27**, 113 (2006).
- 44 D. Silverthorn, *Adv. Physiol. Educ.* **27**, 91–96 (2004).
- 45 G. C. Kim, G. J. Kim, S. R. Park, S. M. Jeon, H. J. Seo, F. Iza, and J. K. Lee, *J. Phys. D: Appl. Phys.* **42**(3), 032005 (2008).
- 46 J. Köritzer, V. Boxhammer, A. Schäfer, T. Shimizu, T. G. Klämpfl, Y.-F. Li, C. Welz, S. Schwenk-Zieger, G. E. Morfill, J. L. Zimmermann, and J. Schlegel, *PLoS One* **8**(5), e64498 (2013).
- 47 Z. Chen, X. Cheng, L. Lin, and M. Keidar, *J. Phys. D: Appl. Phys.* **50**(1), 015208 (2016).
- 48 A. Jo, H. M. Joh, T. H. Chung, and J. W. Chung, *Oxid. Med. Cell. Longevity* **2020**, 4205640.
- 49 R. Sensenig, S. Kalghatgi, E. Cerchar, G. Fridman, A. Shereshevsky, B. Torabi, K. P. Arjunan, E. Podolsky, A. Fridman, G. Friedman, J. Azizkhan-Clifford, and A. D. Brooks, *Ann. Biomed. Eng.* **39**, 674–687 (2010).
- 50 A. V. Ivanov, S. Trakhtenberg, A. K. Bertram, Y. M. Gershenzon, and M. J. Molina, *J. Phys. Chem. A* **111**, 1632–1637 (2007).
- 51 I. G. Zacharia and W. M. Deen, *Ann. Biomed. Eng.* **33**(2), 214–222 (2005).
- 52 N. Srivastava and C. Wang, *J. Appl. Phys.* **110**(5), 053304 (2011).
- 53 L. M. Martini, G. Dilecce, M. Scotoni, P. Tosi, and S. D. Benedictis, *Plasma Processes Polym.* **11**(3), 232–238 (2014).
- 54 J. Winter, M. Dünnbier, A. Schmidt-Bleker, A. Meshchanov, S. Reuter, and K.-D. Weltmann, *J. Phys. D: Appl. Phys.* **45**(38), 385201 (2012).

- ⁵⁵Z. Chen, H. Simonyan, X. Cheng, E. Gjika, L. Lin, J. Canady, J. H. Sherman, C. Young, and M. Keidar, *Cancers* **9**(6), 61 (2017).
- ⁵⁶C. G. Kevil, G. K. Kolluru, C. B. Pattillo, and T. Giordano, *Free Radical Biol. Med.* **51**(3), 576–593 (2011).
- ⁵⁷Z. Chen, L. Lin, X. Cheng, E. Gjika, and M. Keidar, *Biointerphases* **11**, 031010 (2016).
- ⁵⁸D. Dobrynin, G. Fridman, G. Friedman, and A. Fridman, *New J. Phys.* **11**, 115020 (2009).
- ⁵⁹D. Yan, A. Talbot, N. Nourmohammadi, X. Cheng, J. Canady, J. Sherman, and M. Keidar, *Sci. Rep.* **5**, 18339 (2015).
- ⁶⁰R. Dorai and M. J. Kushner, *J. Phys. D: Appl. Phys.* **36**, 666 (2003).
- ⁶¹P. Lu, D. Boehm, P. Cullen, and P. Bourke, *Appl. Phys. Lett.* **110**, 264102 (2017).
- ⁶²T.-J. Fan, L.-H. Han, R.-S. Cong, and J. Liang, *Acta Biochim. Biophys. Sin.* **37**, 719–727 (2005).
- ⁶³H. Adil Ban, M. Al-Shammri Ahmed, and H. Murbat Hamid, *Res. J. Biotechnol.* **14**, 192–195 (2019).
- ⁶⁴A. Petros, A. Medek, D. Nettesheim, D. Kim, H. S. Yoon, K. Swift, E. Matayoshi, T. Oltersdorf, and S. Fesik, *Proc. Natl. Acad. Sci. U. S. A.* **98**, 3012–3017 (2001).
- ⁶⁵S. L. Bailey, K. E. Gurley, K. Hoon-Kim, K. S. Kelly-Spratt, and C. J. Kemp, *Mol. Cancer Res.* **6**(7), 1185 (2008).
- ⁶⁶N. Hawkins, J. Lees, R. Hargrove, T. O'Connor, A. Meagher, and R. Ward, *Tumor Biol.* **18**(3), 146–156 (1997).